Analytical Model for the Performance of a Free-Space Luminescent Solar Concentrator

Geert C. Heres, Lisanne M. Einhaus and Rebecca Saive

Inorganic Material Science, MESA+ Institute, University of Twente, Enschede, the Netherlands

Abstract— *Conventional luminescent solar concentrators suffer from high losses due to the large path length inside the device. Our system reduces these losses by using the free-space to collimate the light. We have developed an analytical model for the performance of those free-space luminescent solar concentrators. Our model takes all loss mechanisms into account and outputs the angle and wavelength dependent emission. Using realistic material parameters, we calculate the intensity emitted by the free space concentrator to be 1.5 times higher than that of a perfect diffuse reflector for all emission angles below 19 degrees.*

Keywords—diffused light, nanophononics, luminescent solar concentrators

I. Introduction

Converting the energy of diffused light optimally is particularly important for often overcast regions and countries. In the Netherlands, for example, more than half of the incident light is diffused [1]. Several solutions to this challenge have been investigated in the past few decades. Most notable are the luminescent solar concentrators (LSCs) first proposed by Weber and Lambe [2]. In these devices, high energy broadband (blue) light is absorbed by luminophores embedded in a waveguide and re-emitted at a lower energy (red-shifted). A large fraction of the light is then trapped due to total internal reflection. Part of the trapped light makes it to the solar modules that are attached to the edges of the LSC (see Fig. 1a). Since the area of the edges is much smaller than the area used to capture the light, the intensity at the edges can be significantly higher than the incoming intensity. However, the trapped light needs to travel a long way through the waveguide. This causes significant losses due to reabsorption, especially for devices with a large concentration factor. To circumvent these issues, we use a nanophotonic system that only allows light to escape in a narrow cone. This mechanism was first described in [3] and is shown schematically in Fig. 1b. While a conventional LSC concentrates the light by decreasing the area, our concept decreases the angular spread instead. I.e., we increase the flux per solid angle instead of the flux per area. This light can be redirected towards existing solar modules to improve their output. Ideally, such a device focuses all incoming light into a narrow cone. However, there are several loss mechanisms that need to be considered, such as the quantum yield of the luminophores and the imperfect reflectance of the bottom surface. Both loss mechanisms have a greater impact the longer the light is trapped inside the structure. The broad emission spectrum of the luminophores and physical limitations of the reflectance properties of the dielectric stack further limit the device performance. The most accurate way to determine the performance is using Monte Carlo simulations. However, those are computationally and time expensive. We developed an analytical model to evaluate the performance of the free-space concentrator using realistic material parameters. This model is derived using linear system theory for the steady state output of the system. Our method is also applicable to conventional LSCs and we were able to reproduce the analytical model from [4]. Here, we first describe the method for the derivation of our model. Then we apply our model with realistic material parameters and compare the results to an ideal Lambertian reflector.

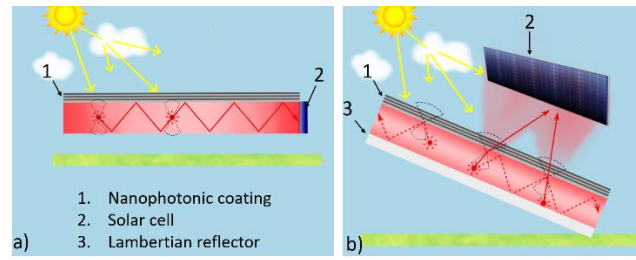

Fig. 1. a) Conventional luminescent solar concentrator and b) free-space solar concentrator with nanophotonic coating, emitting light into a narrow cone, while a Lambertian reflector on the bottom randomizes the direction of the trapped light.

II. The Model

We assume that the light inside the waveguide is isotropic at any point. This is warranted by the fact that the Lambertian reflector randomizes the directions of the light at every reflection on the bottom surface. Furthermore, we assume no anisotropic extinction mechanisms. We also assume that the wavelength does not change after the first emission of the light i.e., subsequent absorption/emission events keep the light at the same wavelength. There are five dominant places where we can define the intensity. These will form five nodes. Node 1 is the intensity of the incoming light, node 2 is the amount of light that is absorbed in the luminophores. Nodes 3 and 4 are the intensities that are incident on the bottom and top surfaces respectively, and node 5 is the emitted light. We set up a photon flow diagram that shows the possible exchanges of energy between these nodes. The parameters that describe these connections are listed in Table 1. The nodes and connections are shown in Fig. 2.

978-1-6654-1922-2/21/$31.00 ©2021 IEEE

Table 1. List of system parameter definitions

P_{R_1}	Angle averaged reflectance of top surface
P_{R_2}	Bottom surface reflectance
η_q	Photoluminescent quantum efficiency
η_{abs}	Absorption efficiency
A_d	Angle-averaged direct re-absorption
A_i	Angle-averaged absorption between top and bottom
f_L	Fraction of light absorbed due to luminophores

When light travels between the top and bottom reflectors, a fraction A_i of this light is absorbed. A_i is calculated by averaging the Lambert-Beer law over the angular distribution of the light. The luminophores can emit the light at any point in the waveguide, A_d is the average absorption of this emitted light over all luminophore positions and emission angles. The host material of the waveguide can also absorb light, this process competes with the luminophore absorption and results in an increase in the absorption coefficient. This increases the total amount of absorbed light. A fraction f_L of this light is absorbed by the luminophores and the rest of the light is lost. The flow diagram of Fig. 2 can be viewed as a linear system in steady state, where each node has a linear equation describing its relation to the other nodes. The terms in these equations are given by the factors on the arrows going into the node. For example, (1) is the equation of node 3.

$$\boldsymbol{I_3} = \frac{1}{2}\eta_q(1-A_d)\cdot \boldsymbol{I_2} + P_{R_1}(1-A_i)\cdot \boldsymbol{I_4} \qquad (1)$$

On the left side of the equation, we have the node itself, and on the right side we see a linear combination of other nodes. Together, the five nodes result in a system of 5 equations that needs to be solved. First, we define a state vector $\boldsymbol{q}$ as a column vector consisting of the intensity of the light present in each node. i.e., $\boldsymbol{q} = [\boldsymbol{I_1}, \boldsymbol{I_2}, \boldsymbol{I_3}, \boldsymbol{I_4}, \boldsymbol{I_5}]$. Then, we can write the system of equations compactly as (2). Finally, the incident light is included in a separate vector $\boldsymbol{b}$ that is added after the matrix multiplication. Light can only enter the system at the top surface, so, $\mathbf{b} = [1, 0, 0, 0, 0]$.

$$\boldsymbol{q} = \boldsymbol{M}\boldsymbol{q} + \boldsymbol{b}, \qquad (2)$$

Where the matrix $\boldsymbol{M}$ is given by:

$$\boldsymbol{M} = \begin{pmatrix} 0 & 0 & 0 & 0 & 0 \\ \eta_{abs} & \eta_q A_d f_L & P_{R_2} A_i f_L & P_{R_1} A_i f_L & 0 \\ 0 & \frac{1}{2}\eta_q(1-A_d) & 0 & P_{R_1}(1-A_i) & 0 \\ 0 & \frac{1}{2}\eta_q(1-A_d) & P_{R_2}(1-A_i) & 0 & 0 \\ 0 & 0 & 0 & 1-P_{R_1} & 0 \end{pmatrix}$$

Now, (2) can be solved to get the state vector,

$$\boldsymbol{q} = (\boldsymbol{M} - \boldsymbol{I})^{-1}\boldsymbol{b}, \qquad (3)$$

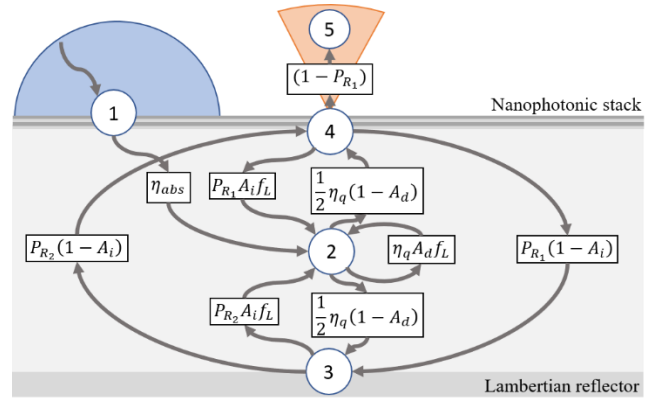

Fig. 2. *Photon flow diagram, each arrow represents the fraction of light that is transferred between nodes.*

This equation allows us to calculate the state vector given the parameters of the system and the input intensity. It was evaluated using the symbolic toolbox in MATLAB, to obtain a functional form of the state vector. Node 4 ($\boldsymbol{I_4}$) is the intensity that is incident on the surface from the inside for a single wavelength. If we multiply this with the normalized luminophore emission spectrum, we find the wavelength dependent intensity that is incident on the top surface $L_{in}(\lambda)$. This, combined with the full knowledge of the transmittance of the top surface $T(\lambda, \theta)$, can be used to calculate the distribution of the transmitted light $L_{out}(\lambda, \theta)$, which is the desired quantity. At first, we will consider a single emission wavelength. Using that solution, it is possible to find the result for the full emission spectrum. We are interested in the angular distribution of the emitted light, not just the total intensity. This distribution is the product of the incident intensity and the transmittance. This results in (4).

$$L_{out}(\lambda, \theta_{out}) = L_{in}(\lambda)\cdot T_{out}(\lambda, \theta_{out})\cdot \frac{1}{n}\frac{d\theta_{in}}{d\theta_{out}}, \qquad (4)$$

Where n is the refractive index and the two angles are related by Snell's law. The final term is needed for the conservation of energy across the surface. Given this solution for a single emission wavelength, the output for a dye with a broader spectrum is given by the product of the single wavelength result and the normalized emission spectrum.

III. Results

To give an example, we will consider a dye with a Gaussian spectrum, emission at 640nm and a FWHM of 50nm. With this spectrum, we can determine which regimes need to have high and low reflectance. The reflectance was simulated using the built-in transfer matrix method of Lumerical. The reflectance was optimized using a particle swarm optimization algorithm on the thicknesses of 26 layers of alternating SiN_x and SiO_2 on a Mempax substrate. The resulting optimized reflection properties are shown in Fig 3. The angle and wavelength dependent reflectance of a fabricated sample with such parameters was measured using a UV-VIS spectrometer and it was found to be in very close agreement with the simulations.

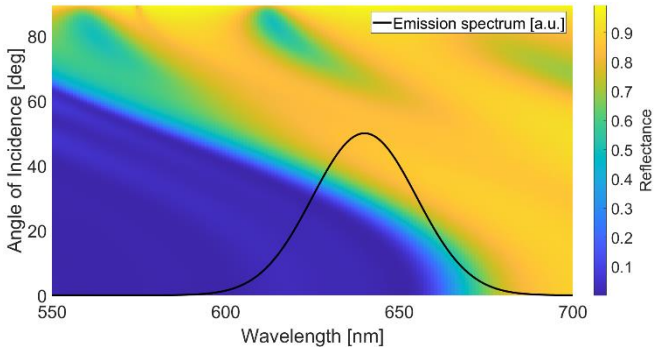

Fig 3: Simulated wavelength and angular dependent reflectance of the dielectric stack for light coming from outside of the structure. The shown reflectance is the average of the TE and TM polarizations. Also shown is the emission spectrum of the example dye.

We consider two sets of system parameters. Firstly, the ideal case, where all loss mechanisms are neglected. In this case, integrating the emission spectrum over all angles and wavelengths should result in one. Then, we consider a realistic case, which shows the potential of this system. The properties of the dye are based on measurements on Lumogen F red dyes done in [4]. The photoluminescent quantum yield is set to 98%, the absorption coefficient and thickness are set such that 95% of the blue light is absorbed. Then, the reabsorption coefficient is set to one tenth of the peak absorption. This results in direct A_d and indirect A_i re-absorption fractions of 22% and 24% respectively. The fraction f_L is set to 0.95, which could be increased by using a higher luminophore concentration. Lastly, the Lambertian reflector is set to 98%, which is a realistic value achieved for example by integrating sphere coatings. With these parameters, we can use (3) to calculate the emission as a function of emission angle and wavelength. The angle and wavelength dependent emission is shown in Fig. 4. Qualitatively, we see that most of the light is emitted inside a cone of 30°, showing that the structure works as intended.

To better show the effectiveness of the structure, we can look at the average output over all emitted wavelengths. This allows comparisons with diffuse reflectors and it gives an idea about the efficiency of the device. The angular emission is shown in Fig. 5. For comparison, the angular distribution of a perfect Lambertian reflector (reflectance of 100%) is also shown. We see that the concentrator achieves 1.5 times higher intensity than an ideal Lambertian reflector for angles smaller than 19 degrees. For the ideal device this extends up to 28 degrees. The ideal structure emits 50.3% at an angle smaller than 30 degrees. The realistic structure in total emits 65% of the incident light, 50.3% of which is confined to 30 degrees. Thus realistically, we can redirect 33% of the incoming diffused light into an emission cone of 30 degrees. Whereas the Lambertian reflector, only reflects 25% into such a cone.

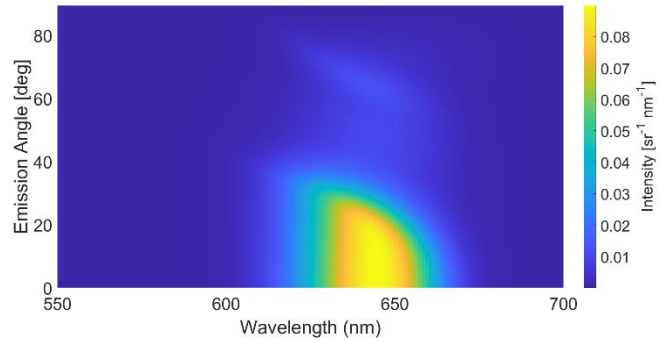

Fig. 4. Light emitted per angle and per wavelength as a function of wavelength and emission angle, normalized to the incoming light. Calculated using the realistic parameters.

IV. CONCLUSION

We have described a free-space solar concentrator that is able to collimate diffused light into an escape cone. This can be used to increase the efficiency of solar modules under diffused light conditions. We presented an analytical model for the emission of this device. This type of model can also be used for conventional solar concentrators. According to our model, the intensity emitted by our device is 1.5 times higher than a perfect Lambertian reflector. In our next steps, we will build and experimentally validate the performance of free-space luminescent concentrators.

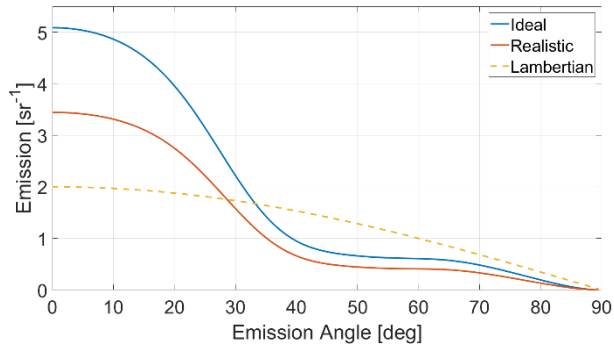

Fig. 5. Angular dependent emission integrated over the emission spectrum.

V. REFERENCES

[1] S. Pal and R. Saive, "Experimental Study of the Spectral and Angular Solar Irradiance," *2019 IEEE 46th Photovoltaic Specialists Conference (PVSC),* pp. 3182--3186, 2019.

[2] W. H. Weber and J. Lambe, "Luminescent greenhouse collector for solar radiation," *Applied optics,* pp. 2299--2300, 1976.

[3] L. M. Einhaus and R. Saive, "Free-space concentration of diffused light for photovoltaics," *2020 47th IEEE Photovoltaic Specialists Conference (PVSC),* pp. 1368--1370, 2020.

[4] L. R. Wilson and B. S. Richards, "Measurement method for photoluminescent quantum yields of fluorescent organic dyes in polymethyl methacrylate for luminescent solar concentrators," *Applied optics,* vol. 48, no. 2, pp. 212--220, 2009.

[5] V. I. Klimov, T. A. Baker, J. Lim, K. A. Velizhanin and H. McDaniel, "Quality factor of luminescent solar concentrators and practical concentration limits attainable with semiconductor quantum dots," *ACS Photonics,* vol. 3, no. 6, pp. 1138--1148, 2016.